Astronomy
&
Astrophysics

A study of bright southern slowly pulsating B stars[*]

III. Mode identification for singly-periodic targets in spectroscopy

P. De Cat[1,2], M. Briquet[2,**], J. Daszyńska-Daszkiewicz[2,3],
M. A. Dupret[4], J. De Ridder[2,**], R. Scuflaire[5], and C. Aerts[2,6]

[1] Royal Observatory of Belgium, Ringlaan 3, 1180 Brussel, Belgium
    e-mail: peter@oma.be
[2] Instituut voor Sterrenkunde, Katholieke Universiteit Leuven, Celestijnenlaan 200 B, 3001 Leuven, Belgium
[3] Astronomical Institute of the Wroclaw University, ul. Kopernika 11, 51-622 Wroclaw, Poland
[4] Instituto de Astrofísica de Andalucía, CSIC, Apdo. 3004, 18080 Granada, Spain
[5] Institut d'Astrophysique et de Géophysique, Université de Liège, Allée du Six Août 17, 4000 Liège, Belgium
[6] Department of Astrophysics, University of Nijmegen, PO Box 9010, 6500 GL Nijmegen, The Netherlands

Abstract. We present the results of the mode identification for a sample of 7 bright southern slowly pulsating B stars showing one pulsation frequency in the $\lambda\lambda$ 413 nm Si II profiles. We combined the results from (1) the method of photometric amplitudes; (2) the moment method; and (3) the amplitude and phase variation across the profile to search for the ℓ and m values of the modes best fitting the data. It is the first time that the applicability of these techniques is tested to a sample of main-sequence g-mode pulsators. Combining the moment method with the amplitude and phase variations across the observed line profile gives an improvement in spectroscopic identification of low degree ℓ g-mode pulsations. Using the variations of the higher order even moments $\langle v^4 \rangle$ and $\langle v^6 \rangle$ of the moment method solutions can also help. For HD 181558, HD 24587, HD 140873 and HD 177863, the photometric and spectroscopic results are compatible and point towards $(\ell, m) = (1, +1)$ sectoral modes. For HD 215573, HD 53921 and HD 92287, the results are inconclusive. Our proposed methodology for mode identification is also applicable to γ Doradus stars.

Key words. stars: early-type – stars: variables: general – stars: oscillations – line: profiles

1. Introduction

Slowly pulsating B stars (hereafter "SPBs") are B-type variables pulsating in high-radial-order g-modes with periods of the order of days. This term was introduced by Waelkens (1991) on the basis of his observational study. Later on, Gautschy & Saio (1993) and Dziembowski et al. (1993) were able to show that the modes observed in the SPBs are excited by the κ mechanism active in the partial ionization layers of the iron-group elements (see also Pamyatnykh 1999 for an extensive review). Townsend (2002) performed a systematic theoretical study, using a non-adiabatic theory, of the expected photometric characteristics of SPBs and compared these with the observed characteristics of our work (De Cat 2001). This led him to suggest that SPBs are most likely expected to oscillate in dipole ($\ell = 1$) modes. A similar theoretical prediction for the line-profile variability of SPBs is, to our knowledge, not

available. We treat the particular question of mode identification from the observational side in this work.

This paper is one in a series of papers devoted to the detailed analysis of time-series of Geneva photometry and high-resolution, high signal-to-noise line profiles of the $\lambda\lambda$ 413 nm Si II doublet of the sample of 17 bright southern (candidate) SPBs introduced by Aerts et al. (1999). For a full description of the observations and the data reduction, we refer to Sect. 2 of Paper I (De Cat et al. 2000). Paper I was devoted to the determination of the orbital parameters and the dominant intrinsic frequency of the spectroscopic binaries in the original sample. For HD 69144, no periodic variations are found although it exhibits clear line profile variations. HD 169978, HD 55522 and HD 131120 were misclassified as SPBs (see also Briquet et al. 2001; Briquet et al. 2004). The data sets of the remaining 13 targets were subjected to a detailed frequency analysis in Paper II (De Cat & Aerts 2002). In Paper III (this paper) and Paper IV (De Cat et al. 2005), we discuss the mode identification for targets for which respectively one and more than one pulsation mode is observed in the line profile variations. Since the knowledge of the correct values of the degree ℓ and the azimuthal number m of the excited modes is the starting-point

---

[*] Based on observations collected with the CAT Telescope of the European Southern Observatory and with the Swiss Photometric Telescope of the Geneva Observatory, both situated at La Silla in Chile.

[**] Postdoctoral Fellow of the Fund for Scientific Research, Flanders.

of any asteroseismic study, we based our conclusions on the results of several photometric and spectroscopic identification techniques. Most of these techniques were originally developed for main-sequence *p-mode* pulsators while they are here applied to main-sequence *g-mode* pulsators.

While the excitation mechanism of main-sequence B stars is relatively well understood in global terms, open questions remain for particular modes in selected stars. An example of this can be found for the β Cep star ν Eri, for which Pamyatnykh et al. (2004) and Ausseloos et al. (2004) performed detailed seismic modeling. One of the large-amplitude modes observed in this star, the $\ell = 1$, p_2 mode, is not excited by current models with a solar mixture. An increase in the iron abundance with a factor at least four, either in the driving layer or in the star as a whole, is necessary to achieve the excitation of that particular mode. Given that such delicacies turn up when treating specific targets, we have chosen not to take the vibrational stability of the observed pulsation modes into account as a constraint on the mode identification in this work. We refer to an additional paper in this series, Paper V (Daszyńska-Daszkiewicz 2005) for a fully detailed discussion of stability analyses for the SPBs and its implication for mode identification.

This paper is organized as follows. In Sect. 2, we describe the identification procedure used to find the ℓ and m values in this paper and in Paper IV. In Sect. 3, the individual results of our targets with one observed pulsation mode in spectroscopic data are discussed. We first give a summary of the results in Sect. 3.8 before ending with our conclusions and a discussion in Sect. 4.

2. Identification procedure

Consider an SPB star from our sample. Let N denote the total number of pulsation frequencies found for this star in our current data sets, and N_s the number retained in the variations of the Si II line profiles. The stars with $N_s = 1$ are subject of this paper, and those with $N_s > 1$ of Paper IV. The aim of the identification procedure is to find the degrees ℓ_j and the azimuthal numbers m_j of the modes corresponding to the observed intrinsic frequencies $\nu_{j,\text{obs}}$ (see Tables 2–15 of Paper II) with $j = 1, ..., N$.

2.1. Approximations

All the mode identification methods that we have used in this work suffer from restrictive assumptions regarding the stellar rotation, which may become critical for SPBs. Indeed, to interpret gravity modes as occur in SPBs and γ Doradus stars, the effects of rotation may become important and one has to check a posteriori if the assumptions made are justified. In particular, we did not take into account the effects of the centrifugal force in any of our analyses. The justification of this can be checked by computing the ratio of the equatorial rotation velocity v_{eq} to the critical velocity of the star v_{crit}, because this is a measure for the star's deviation from spherical symmetry. As long as this ratio remains below, let's say 20%, the oblateness of the star and the resulting Von Zeipel effect can safely be ignored. On the other hand, an approximation of more concern for
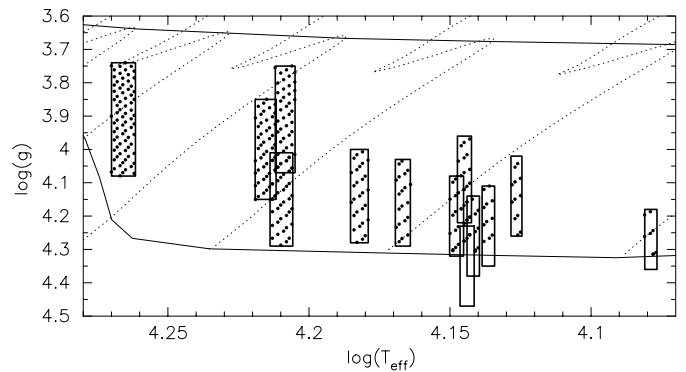

Fig. 1. The dots denote the main-sequence stellar models with $(Z, X) = (0.02, 0.70)$ and no convective overshooting which are compatible with the observed ranges of $\log(T_{\text{eff}})$ and $\log(g)$ (bold lines) for the stars in our sample. The thin lines denote the boundaries of the theoretical SPB instability strip for modes with $\ell \leq 2$ computed using the OPAL opacities (Pamyatnykh 1999). The dotted lines denote evolution tracks for stars with $M = 8$ (*upper left*), 7, 6, 5, 4, 3 $M_\odot$ (*lower right*).

gravity modes is the neglect of the Coriolis force in the theoretical treatment of the oscillations for the mode identification – see Townsend (2003) for a clear and thorough discussion of this problem in the case of mode identification from photometric amplitude ratios. From Fig. 5 in Townsend (2003) one can deduce that the so-called "spin parameter" η, i.e. twice the ratio of the rotation frequency ν_Ω and the oscillation frequency in the co-rotating frame ν_{co}, must remain below 1 in order to be able to safely ignore the Coriolis force in photometric mode identification from amplitude ratios. We have indeed ignored the effect of the Coriolis force in our photometric mode identifications, but we did take this force into account in the spectroscopic identifications. This allows us, after final mode identification and derivation of the rotation frequency from the spectroscopic variations, to test if the neglect of the Coriolis force in treating the photometry was justified.

2.2. Photometric identification procedure

In a first step, the most probable values for the degrees ℓ_j are found by applying the method of photometric amplitudes (using the formalism of Dupret et al. 2003) to the observed variations in Geneva data – see also Townsend (2002). Let $A^X_{j,\text{obs}}$ denote the amplitude of the observed variations with pulsation frequency $\nu_{j,\text{obs}}$ in filter $X \in \{U, B_1, B, B_2, V_1, V, G\}$ of the Geneva photometric system. We used CLES (version 13, code written by R. Scuflaire) to calculate stellar models for main-sequence stars with masses ranging from 2 to 8 $M_\odot$ in steps of 0.1 $M_\odot$ assuming solar metalicity ($Z = 0.020$), initial hydrogen abundance $X = 0.70$, and no convective overshooting. For every star in our sample, we selected the models whose T_{eff} and $\log(g)$ are situated within the observed boxes as given in Table 1 of Paper II (see Fig. 1, "error box models"). Next, we calculated the non-adiabatic eigenfunctions and eigenfrequencies for g-modes with $\ell_j \leq 3$ by using MAD (code written by M.-A. Dupret). For each error box model, we searched for each ℓ_j the mode whose eigenfrequency is the closest to the

observed pulsation frequency $\nu_{j,\text{obs}}$ to calculate the corresponding theoretical amplitude ratios $A_{j,t}^X(\ell)/A_{j,t}^U(\ell)$. Our assumption that the observed frequency is equal to the one in the co-rotating frame is only valid for $m_j = 0$ modes and was checked a posteriori (see Sect. 3.8). For each ℓ_j, the resulting theoretical amplitude ratios were compared to the observed photometric amplitude ratios and their standard errors to select the best fitting ℓ_j value.

2.3. Spectroscopic identification procedure

In a second step, the moment method was applied to line profiles of the $\lambda\lambda$ 413 nm Si II doublet. The discriminant compares the observed normalized moments $\langle v \rangle$, $\langle v^2 \rangle$ and $\langle v^3 \rangle$ to theoretical ones (Aerts et al. 1992). Since the two Si II lines generally lead to similar results, we here restrict ourselves to the Si II line that was selected in Paper II for the frequency analysis. We follow the approach of Briquet & Aerts (2003), who use the BRUCE code of Townsend (1997) based on the formalism of Lee & Saio (1987). We used both the versions (not) including the effects of the Coriolis force in the traditional approximation (see Townsend 1997) and will refer to these as "moment method with the (non-)rotating pulsation formalism". The criterion described in Sect. 2.5 of Briquet & Aerts (2003) allowed us to restrict our grids to $1 \leq \ell_j \leq 3$. We varied the "continuous parameters", i.e. the inclination $0° \leq i \leq 90°$ in steps of $1°$, the projected rotation velocity $0 \text{ km s}^{-1} \leq v_\Omega \leq v_{\text{tot}}$ in steps of 1 km s^{-1} (with v_{tot} the total broadening of the line profile), and the intrinsic width of the considered line profile $1 \text{ km s}^{-1} \leq \sigma_\lambda \leq 20 \text{ km s}^{-1}$ in steps of 1 km s^{-1}. For each $(l_j, m_j, i)_{j=1}^{N_s}$ combination, the value for the amplitude of the radial part of the pulsation velocity $(A_{\text{p},j})_{j=1}^{N_s}$ was fixed such that the theoretical amplitude of $\langle v \rangle$ matches the observed one (Tables 2–15 of Paper II). To a good approximation, the ratio of the tangential to radial component of the pulsation velocity is given by:

$$K_j = \frac{GM}{4\pi^2 \nu_{j,\text{co}}^2 R^3} = \frac{GM}{4\pi^2 (\nu_{j,\text{obs}} + m_j \frac{v_\Omega}{2\pi R \sin i})^2 R^3}, \qquad (1)$$

where $\nu_{j,\text{co}}$ is the pulsation frequency in the co-rotating frame. For each (m_j, v_Ω, i) combination, we used the K_j value found with the mass M, the radius R and $\nu_{j,\text{obs}}$ as given in Tables 1–15 of Paper II. The error on K_j due to large uncertainties on the mass and the radius does *not* influence the mode identification (Briquet & Aerts 2003). The linear limb darkening coefficient u was found by interpolation in the grid of Wade & Rucinski (1985) for solar abundance models. For each $(\ell_j, m_j)_{j=1}^{N_s}$ combination, the best fitting i, v_Ω and σ_λ values are found by minimizing the discriminant. Unfortunately, the resulting $\gamma(\ell_j, m_j)_{j=1}^{N_s}$ values generally do not differ much (Tables 1–7).

The BRUCE/KYLIE codes (Townsend 1997) were used in a third step to calculate synthetic profiles corresponding to the first "few" deepest minima of both versions of the moment method. Since the stellar distortion and the Von Zeipel effect are neglected in the calculations of the discriminant of both versions of the moment method, they were also not considered here. We calculated for both the observed and

synthetic line profiles up to $\langle v^6 \rangle$ to make phase plots with $\nu_{j,\text{obs}}$, from which some solutions could be excluded. Next, we calculated the "IPS diagnostics", i.e. the amplitudes and phases of variations with $\nu_{j,\text{obs}}$ and $2\nu_{j,\text{obs}}$ across the line profile (cf. Schrijvers et al. 1997; Telting & Schrijvers 1997; Telting et al. 1997). The IPS method was designed for studying p-modes. Numerous simulations for higher degree modes ($\ell > 3$) in rapidly rotating stars ($v_\Omega > 5\sigma_\lambda$) under the assumption that $v_\Omega \ll v_{j,\text{obs}}$ led to empirical relations between ℓ, m and the total phase difference of respectively $\nu_{j,\text{obs}}$ and $2\nu_{j,\text{obs}}$ across the line profile. Since these assumptions are generally not valid for SPBs, Eqs. (9) and (10) of Telting & Schrijvers (1997) cannot be used here. However, a direct comparison of the synthetic and observed amplitude and phase variations across the line profile enabled us to pinpoint the best fitting spectroscopic solutions. For clarity, only the phase variations with $\nu_{j,\text{obs}}$ are shown. These phase curves were shifted such that the bluest considered wavelength has phase $= 0$. Moreover, they are corrected for phase jumps of 2π such that the phase difference between 2 adjacent wavelengths never exceeds π. This choice of correction might, in some cases, introduce unexpected phase jumps.

2.4. Combined results

Finally, the results of the photometric and spectroscopic identification procedure are combined to identify the overall best fitting ℓ_j and m_j values of the observed modes. In case of a successful identification, the values of the continuous parameters found with the moment method can, in principle, be used to derive e.g. the rotation frequency ν_Ω. However, De Ridder et al. (2004) showed that the errors on the projected rotation velocity v_Ω and especially on the inclination i are in general too high to be useful for such purposes in the mono-periodic case.

3. Results of the mode identification

In the following subsections, we present the results of the identification procedure for a subsample of the targets of Aerts et al. (1999) consisting of SPBs with only one observed pulsation mode in the spectroscopic data.

3.1. HD 181558 – HR 7339 – HIP 95159

Although HD 181558 ($m_V = 6.24$, B5III, $v_{\text{tot}} \simeq 25 \text{ km s}^{-1}$) is known as a multi-periodic SPB (Waelkens 1991), only one dominant frequency, i.e. $\nu_1 = 0.80780(10) \text{ c d}^{-1}$, could be determined without ambiguity with our data sets (Paper II).

The large amount of measurements in the Geneva photometric system allowed an accurate determination of the amplitudes and phases of the variations with ν_1 (Table 7 of Paper II). The theoretical amplitude ratios for relevant ℓ_1 values found from the error box models are not compatible with the observed amplitude ratios (Fig. 2), although the lines for $\ell_1 = 1$ are quite close to the observed ratios. Hence $\ell_1 = 1$ is the best fitting photometric identification. The small discrepancy could be due to a different value of the metalicity and/or the overshooting parameter than the one we adopted.
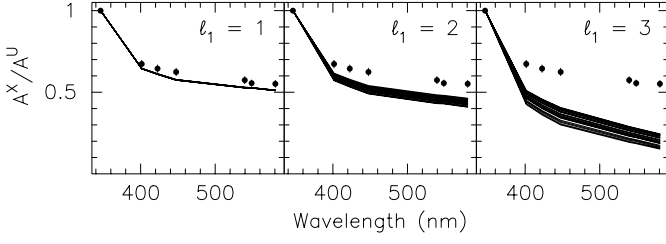
Fig. 2. Photometric mode identification for $\nu_1 = 0.80780(10)$ c d^{-1} of HD 181558. For each theoretical model within the observed range of $\log(T_{\text{eff}})$ and $\log(g)$ (cf. Fig. 1), the theoretical amplitude ratios for modes with $\ell_1 = 1$ (*left*), 2 (*middle*), and 3 (*right*) are represented with an individual line. The dots indicate the observed amplitude ratios and their standard error.
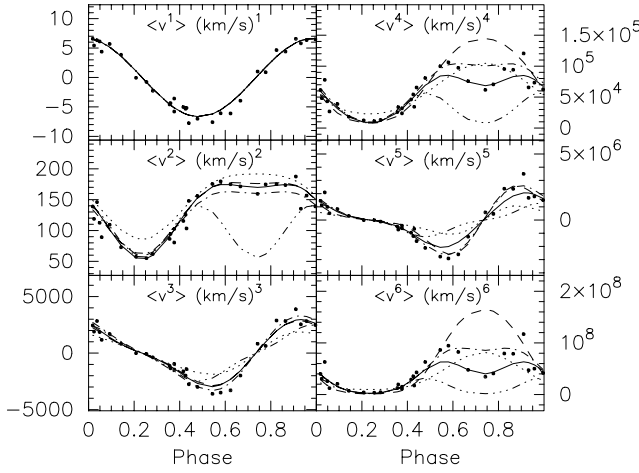

Fig. 3. The observed (dots) and theoretical (lines) moments corresponding to the 5 best fitting solutions found with the identification code without inclusion of the Coriolis force (Briquet & Aerts 2003) for the mode with frequency ν_1 of HD 181558 (cf. upper part of Table 1). The full, dashed, dot-dashed, dotted and dashed-dot-dot-dot line denote respectively solution 1–5.

The 5 best fitting solutions found with the moment method are given in Table 1. Since HD 181558 is the star with the narrowest lines in our subsample, we expect only small differences in the results of both versions of the moment method. Indeed, although the solutions are found in a different order, the differences in the values of $\gamma(\ell_1, m_1)$ and the continuous parameters are quite small. In both cases, there are 3 solutions, i.e. with $(\ell_1, m_1) = (1, +1)$, $(2, -1)$ and $(2, -2)$, whose discriminant values are close to each other and much lower than for the other solutions. This is reflected in Fig. 3 where we show phase plots with ν_1 of the observed moments up to $\langle v^6 \rangle$ and of the 5 best fitting solutions of the moment method with the *non-rotating* pulsation formalism (Table 1, top rows). Considering $\langle v \rangle$, $\langle v^2 \rangle$ and $\langle v^3 \rangle$ implies that solutions 1 (solid line), 2 (dashed line) and 3 (dot-dashed line) are better than solutions 4 (dotted line) and 5 (dashed-dot-dot-dot line). When looking at $\langle v^4 \rangle$ and $\langle v^6 \rangle$, it is also clear that solution 2 (dashed line) is not a good one. The IPS diagnostics shown in Fig. 4 for the remaining best fitting solutions 1 and 3 clearly point towards $(\ell_1, m_1) = (1, +1)$ as the best fitting spectroscopic identification. The results of the moment method *with the rotating pulsation formalism* lead to
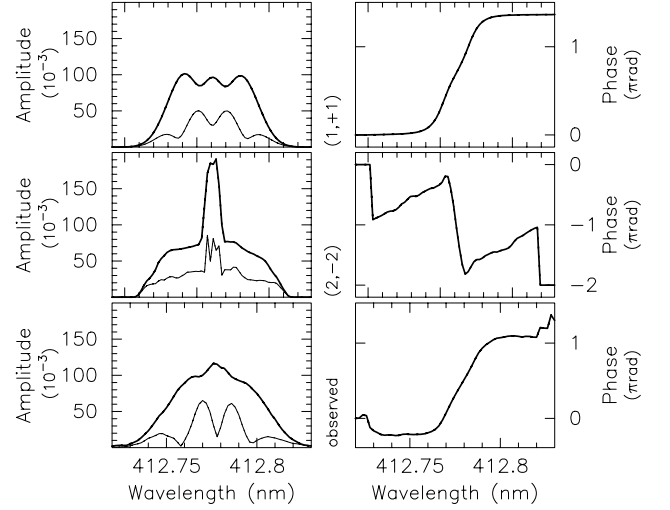

Fig. 4. IPS diagnostics for observed and synthetic Si II profiles corresponding to the (two) best fitting identifications for ν_1 of HD 181558 from the moment method with the non-rotating pulsation formalism (top rows of Table 1). We show the amplitude (*left*) and phase (*right*) of variations with ν_1 (bold line) and $2\nu_1$ (thin line) across the profiles. The phase curves are corrected for phase jumps of 2π and shifted such that the bluest considered wavelength has phase = 0.

Table 1. The five best fitting solutions found with the moment method without (*top*) and with (*bottom*) inclusion of the Coriolis force (Briquet & Aerts 2003) for the mode varying with ν_1 of HD 181558. We list the degree ℓ_1, the azimuthal number m_1, the discriminant value $\gamma(\ell_1, m_1)$ (km s^{-1}), the amplitude of the radial part of the pulsation velocity $A_{p,1}$ (km s^{-1}), the maximum radial and tangential surface velocities $v_{r,\text{max}}$ (km s^{-1}) and $v_{t,\text{max}}$ (km s^{-1}), the ratio of the tangential to radial component of the pulsation velocity K_1, the inclination angle i (°), the projected rotation velocity v_Ω (km s^{-1}), and the intrinsic width σ_λ (km s^{-1}) of the considered $\lambda = 413.0$ nm Si II line. "$\ll$" and "$\gg$" indicates values of respectively <0.01 and >1000.

n°	ℓ_1	m_1	$\gamma(\ell_1, m_1)$	$A_{p,1}$	$v_{r,\text{max}}$	$v_{t,\text{max}}$	K_1	i	v_Ω	$\sigma_{413.0}$
1	1	+1	7.70	3.50	1.21	19.73	16	42	12	7
2	2	−1	7.75	0.59	$\ll$	31.73	70	16	14	1
3	2	−2	7.95	0.62	0.24	26.33	55	53	17	1
4	3	−2	9.74	1.08	$\ll$	32.44	29	62	7	4
5	1	0	9.85	2.20	$\ll$	23.41	22	55	13	4
	2	−1	7.52	0.50	$\ll$	20.64	44	34	19	2
	1	+1	7.77	4.75	1.65	27.52	17	25	7	3
	2	−2	7.98	0.87	0.34	35.70	52	48	15	1
	3	−1	9.73	0.55	0.19	7.74	40	30	15	4
	3	−2	9.82	1.12	$\ll$	32.40	28	60	6	5

the same final conclusion. This is also true for the other stars in this subsample, although some of the proposed solutions with the rotating pulsation formalism are not realistic (e.g. for HD 140873 in Table 3: too high K-values). The figures corresponding to the results of the moment method with the rotating pulsation formalism are therefore not shown.

We conclude that the photometric and spectroscopic mode identification are compatible with each other. We are therefore confident that we are dealing with an $\ell_1 = 1$ sectoral mode.
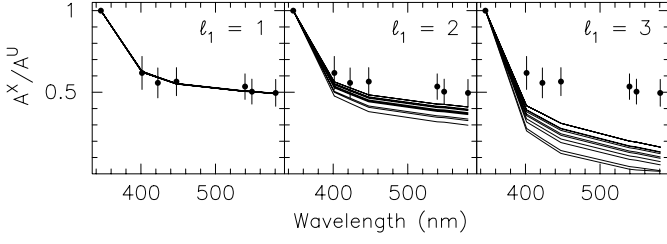
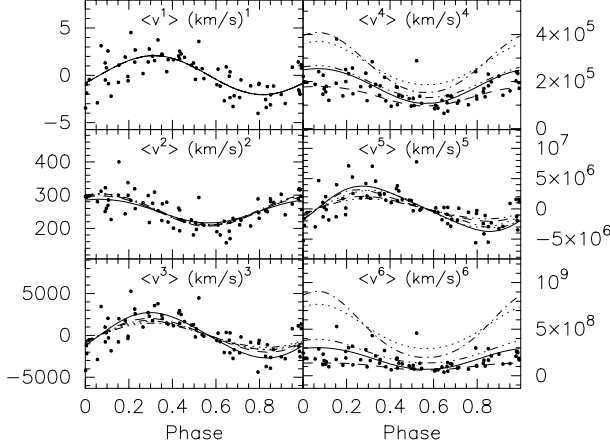**Fig. 5.** Same as Fig. 2, but for $\nu_1 = 1.1569(6)$ c d^{-1} of HD 24587.

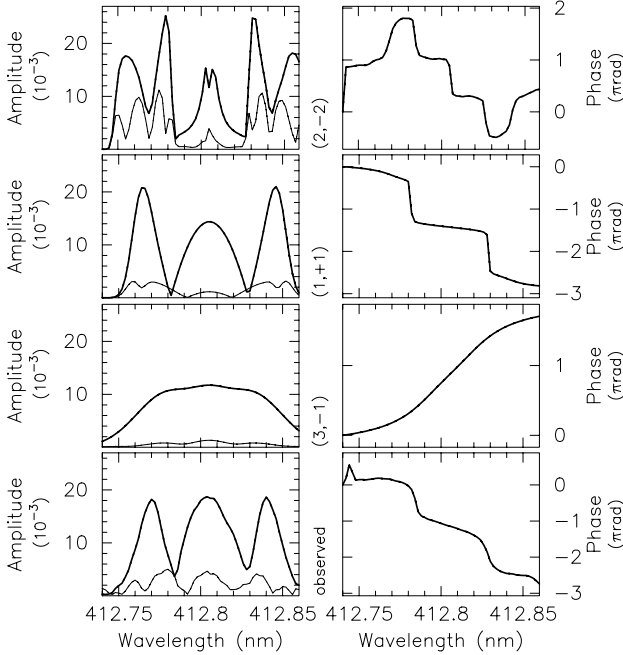

Fig. 6. Same as Fig. 3 but for ν_1 of HD 24587.

Fig. 7. Same as Fig. 4 but for ν_1 of HD 24587.

Table 2. Same as Table 1, but for ν_1 of HD 24587.

n°	ℓ_1	m_1	$\gamma(\ell_1, m_1)$	$A_{p,1}$	$v_{r,max}$	$v_{t,max}$	K_1	i	v_Ω	$\sigma_{412.8}$
1	2	−2	11.14	0.47	0.18	69.19	189	16	14	1
2	1	+1	11.19	2.28	0.79	6.26	8	38	32	3
3	2	−1	11.32	0.03	≪	50.11	≫	3	7	8
4	3	−2	11.34	1.68	0.01	56.92	33	15	6	2
5	3	−1	11.46	0.34	0.11	3.53	32	17	13	14
	2	−2	11.05	0.32	0.16	101.92	315	19	18	12
	3	−1	11.10	0.13	0.06	2.14	38	37	32	2
	2	−1	11.12	0.09	≪	11.64	68	25	32	3
	3	−2	11.23	2.00	0.02	60.35	28	15	5	2
	1	+1	11.28	1.49	0.53	4.47	8	42	31	5

theoretical $\ell_1 = 1$ amplitude ratios obtained with the error box models (Fig. 5, left). The five deepest minima $\gamma(\ell_1, m_1)$ of the discriminant of both versions of the moment method all correspond to non-zonal modes, of which an $\ell_1 = 2$ sectoral mode *appears* as the most probable one (Table 2). After looking at the moment variations, only solution 1, 2 and 5 remain (Fig. 6) of which the $(\ell_1, m_1) = (1, +1)$ solution is clearly the best fitting one according to the IPS diagnostics (Fig. 7). Like for HD 181558, we can conclude that we are dealing with an $\ell_1 = 1$ sectoral mode. Note that the differences between the adopted identifications found with both versions of the moment method are again small (Table 8).

3.3. HD 140873 − HR 5863 − HIP 77227

HD 140873 ($m_V = 5.39$, B8III, $v_{tot} \simeq 75$ km s^{-1}) is a double-lined spectroscopic binary with an orbit of about 39 days with an extremely high eccentricity $e = 0.731(6)$ (Paper I). In most orbital phases, the weak, sharp Si II profiles of the secondary are superposed on the broad Si II profiles of the primary. This handicaps the spectroscopic identification of the mode with frequency $\nu_1 = 1.1515(8)$ c d^{-1} present in all our data sets (Paper II).

The observed Geneva amplitudes of variations with ν_1 used for the photometric identification are given in Table 3 of Paper II. The error box models favor $\ell_1 = 1$ modes (Fig. 8). With the moment method, we find all kinds of modes (Table 3). Note the large differences between the values for the continuous and other parameters of the versions with the rotating and non-rotating pulsation formalism. In the results of the moment method with the rotating pulsation formalism, the proposed $(\ell_1, m_1) = (1, +1)$ mode is the only one with a realistic K_1 value. The high order moment variations with the non-rotating pulsation formalism reveal that solution 3 in Table 3 is not a good one (Fig. 9). Moreover, the $(\ell_1, m_1) = (1, +1)$ solution is here the only one for which the amplitude variations across the 412.8 nm Si II profiles look similar to the observed ones (Fig. 10, left panels). Note the clear difference between the synthetic and observed phase behavior (Fig. 10, right panels). We suspect that these differences are partly due to the pollution of the profiles with those of the secondary component. We will try to improve our results in the future by first disentangling
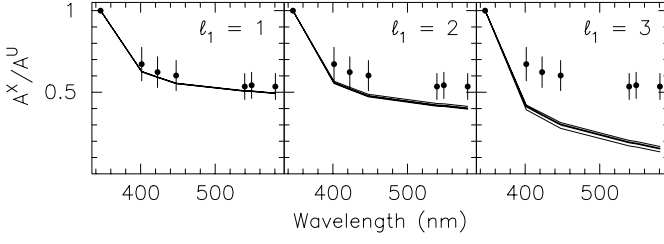
3.2. HD 24587 − HR 1213 − HIP 18216

For HD 24573 ($m_V = 4.63$, B5V, $v_{tot} \simeq 40$ km s^{-1}), one frequency $\nu_1 = 1.1569(6)$ c d^{-1} is commonly present in all our data sets (Paper II). For this mode, the photometric and spectroscopic identification procedures lead to compatible results. A very good correspondence is found between the observed amplitude ratios (derived from Table 4 of Paper II) and the

Fig. 8. Same as Fig. 2, but for $\nu_1 = 1.1515(8)$ c d^{-1} of HD 140873.
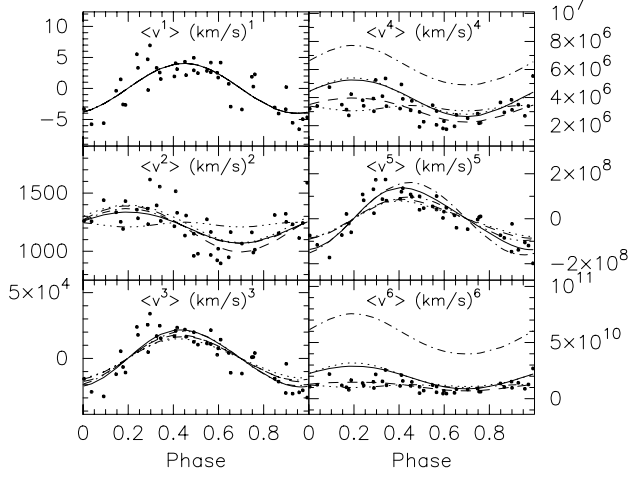
Fig. 9. Same as Fig. 3 but for ν_1 of HD 140873.

Table 3. Same as Table 1, but for ν_1 of HD 140873.

$n°$	ℓ_1	m_1	$\gamma(\ell_1, m_1)$	$A_{p,1}$	$v_{r,max}$	$v_{t,max}$	K_1	i	v_Ω	$\sigma_{412.8}$
1	2	−2	21.14	2.79	1.08	152.07	71	15	25	9
2	1	+1	21.40	7.70	2.66	13.61	5	31	69	8
3	3	−2	21.77	0.88	≪	126.89	141	14	9	3
4	2	−1	22.11	0.66	≪	20.27	40	15	60	19
5	2	0	22.23	0.85	0.27	0.27	22	38	71	5
	2	−1	20.47	≪	≪	81.33	936	34	59	16
	2	−2	21.34	≪	≪	≫	≫	77	61	18
	1	+1	21.40	14.73	5.50	50.39	9	6	7	12
	3	−2	21.41	≪	≪	193.57	≫	53	46	15
	3	−3	21.42	0.05	0.04	33.91	284	45	37	20

the spectra of both components by means of the KOREL code (Hadrava 1995, 1997) before re-analyzing the intrinsic variations of the primary. Note that another choice of corrections with phase jumps of 2π near 412.27 nm and 412.82 nm already results in phase variations which are more similar to the observed ones (dotted line in Fig. 10).

Given the compatibility of the photometric and spectroscopic results, we are confident that we are dealing with an $\ell_1 = 1$ sectoral mode.

3.4. HD 177863 – HR 7241 – HIP 93887

HD 177863 ($m_V = 6.28$, B8V, $v_{tot} \simeq 75$ km s^{-1}) is a single-lined spectroscopic binary with a very eccentric orbit with $\nu_{orb} = 0.083925(6)$ c d^{-1} (Paper I). It is one of the targets in
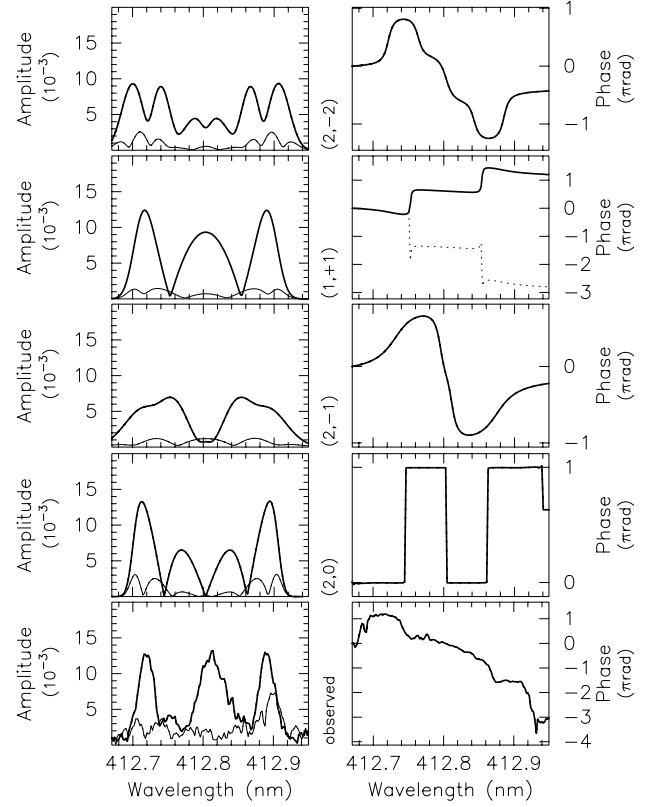

Fig. 10. Same as Fig. 4 but for ν_1 of HD 140873.

the SPB discovery paper of Waelkens (1991) for which we retained two intrinsic frequencies from our current data sets: $\nu_1 = 0.84059(10)$ c d^{-1} and $\nu_2 = 0.10108(10)$ c d^{-1} (Paper II). Note that ν_1 is close to ten times the orbital frequency ν_{orb}. Willems & Aerts (2002) suggested that this mode is a resonantly excited $\ell_1 = 2$ sectoral mode through the time-varying tidal potential. The origin of variations with an *observed* frequency as low as ν_2 is not immediately clear. If it is a pulsation mode, a *high* and *positive* m_2 value is required for the corresponding oscillation frequency in the co-rotating frame to be situated in the expected range of SPB frequencies. However, since ν_2 was not found in the variations of the Si II profiles, we restricted ourselves to the identification of the mode with ν_1 only.

The large amount of measurements in the Geneva photometric system allowed an accurate determination of the amplitudes and phases (Table 8 of Paper II). The observed amplitude ratios agree with those of the error box models with $\ell_1 = 1$ only (Fig. 11). The results of the moment method behave similar to those of HD 140873 (Table 4). Of the solutions with the rotating pulsation formalism, the $(\ell_1, m_1) = (1, +1)$ mode is the first one with a realistic K_1 value. Of the solutions with the non-rotating pulsation formalism, the $(\ell_1, m_1) = (1, +1)$ mode is the only one for which both the variations in the higher order moments (Fig. 12) and the amplitude variations across the 413.0 nm Si II profiles (Fig. 13) mimic the observed ones. Here, another choice of corrections with phase jumps of 2π near 413.04 nm and 413.14 nm is needed for the phase variations to look like the observed ones (dotted line in Fig. 13).
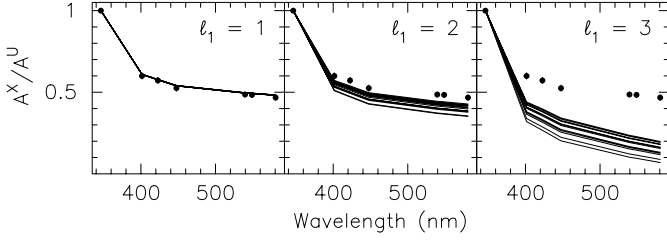
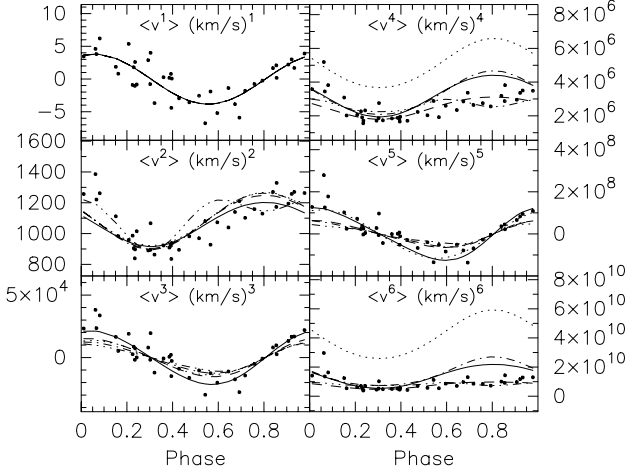**Fig. 11.** Same as Fig. 2, but for $\nu_1 = 0.84059(10)$ c d^{-1} of HD 177863.

Fig. 12. Same as Fig. 3 but for ν_1 of HD 177863.

Fig. 13. Same as Fig. 13 but for ν_1 of HD 177863.

Table 4. Same as Table 1, but for ν_1 of HD 177863.

n°	ℓ_1	m_1	$\gamma(\ell_1, m_1)$	$A_{p,1}$	$v_{r,max}$	$v_{t,max}$	K_1	i	v_Ω	$\sigma_{413.0}$
1	2	−2	19.37	6.64	2.56	143.41	28	15	28	5
2	1	+1	20.16	8.12	2.80	12.64	5	31	67	4
3	2	−1	20.51	1.78	0.01	25.46	18	11	52	20
4	3	−2	20.52	0.23	≪	120.32	443	14	11	1
5	3	−1	20.88	0.40	0.13	13.74	108	72	63	3
	2	−1	19.05	≪	≪	69.14	838	41	65	1
	3	−3	19.29	≪	≪	250.23	≫	63	34	20
	2	−2	19.51	≪	≪	10.39	693	77	66	1
	3	−2	19.62	≪	≪	149.55	≫	44	37	20
	3	−1	19.97	0.05	0.04	5.01	126	40	45	20
	1	+1	20.19	15.63	5.89	46.85	8	6	7	10

Given the agreement with photometry, we conclude that we are dealing with an $\ell_1 = 1$ sectoral mode. Our identification clearly does *not* confirm the scenario of tidal resonance suggested by Willems & Aerts (2002).

3.5. HD 215573 – HR 8663 – HIP 112781

HD 215573 ($m_V = 5.35$, B6IV, $v_{tot} \simeq 30$ km s^{-1}) is one of the few normal mid-B type stars with very sharp spectral lines which makes it an ideal target for abundance studies (Adelman et al. 1993). In Paper II, we found two intrinsic frequencies: $\nu_1 = 0.5439(6)$ c d^{-1} and $\nu_2 = 0.5654(6)$ c d^{-1}. The frequency separation between ν_1 and ν_2 is small, which might indicate that they are part of a frequency multiplet. Since the variations
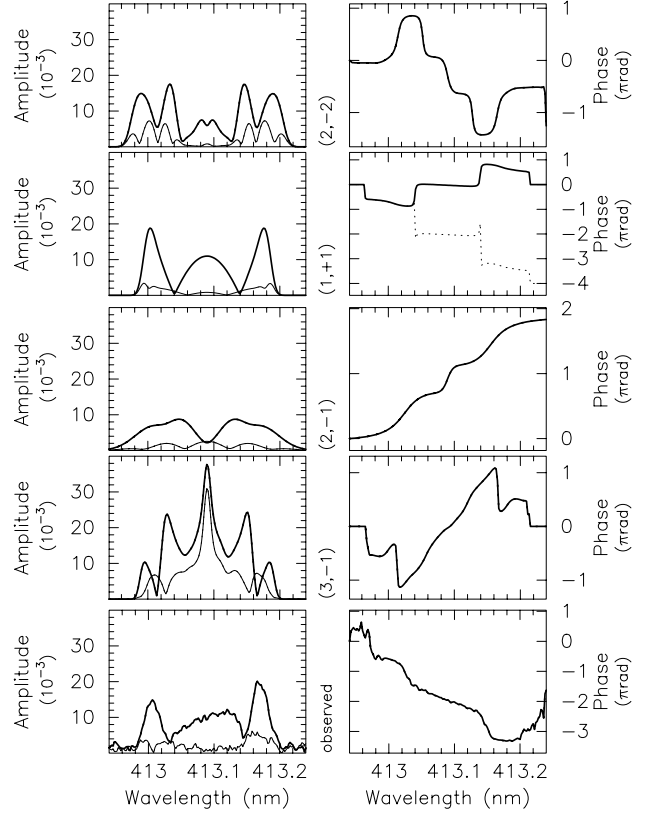
with ν_1 were only found in the H_p-magnitudes, we are only able to conduct a mode identification for the mode with ν_2.

For the photometric identification, we used the observed amplitudes and phases as given in Table 15 of Paper II. For the theoretical amplitude ratios found from considering the error box models, the best agreement is obtained for $\ell_2 = 1$ modes with ν_2 although $\ell_2 = 2$ is also inside the observational error bars and cannot be ruled out (Fig. 14).

Unfortunately, the results of the spectroscopic identification procedure are inconclusive. In Table 5, the 5 best fitting solutions found with both versions of the moment method are listed. We additionally added the best fitting $\ell_2 = 1$ solution. Note that the continuous parameters of the best fitting solutions with the same (ℓ_2, m_2) values are almost exactly the same for both versions of the moment method (Table 5). Moreover, the total difference in discriminant values of *all* solutions are in both cases negligible ($\Delta\gamma(\ell_2, m_2) \simeq 0.09$). Consulting the variations in higher order moments does not help us (Fig. 15). The IPS diagnostics (Fig. 16) suggest that the best overall spectroscopic solution has $(\ell_2, m_2) = (3, -1)$ since it is the only solution for which the phase variations (right panels) resemble the observed ones. However, *none* of *all* the other solutions can be ruled out since the phase jump near 413.12 nm is (almost) exactly π in all cases. Hence, we cannot find a certain identification for this mode.
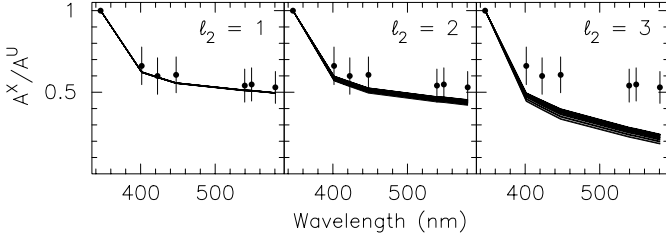
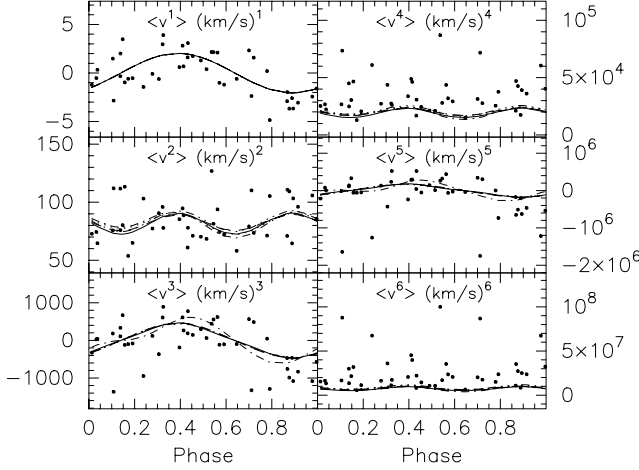**Fig. 14.** Same as Fig. 2, but for $\nu_2 = 0.5456(6)$ c d^{-1} of HD 215573.

Fig. 15. Same as Fig. 3 but for ν_2 of HD 215573.

3.6. HD 53921 – HR 2674 – HIP 34000

HD 53921 (m_V = 5.64, B9IV, $v_{tot} \simeq 50$ km s^{-1}) is known as a close visual binary with two similar B-type components (Corbally 1984). Our observed Si II profiles result from a superposition of the profiles of both visual components, and one of these two visual components is a spectroscopic binary with an eccentric orbit of about 340 d (Paper II). This superposition hampers the identification of the mode with frequency $\nu_1 = 0.6054(6)$ c d^{-1} which is observed in all our data sets. Indeed, the observed amplitude ratios (derived from Table 6 of Paper II) do not follow the expected trends of theoretical amplitude ratios (Fig. 17). The results of both versions of the moment method are almost identical (Table 6). However, the moment method comes up with solutions with v_Ω close to 0 km s^{-1} or v_{tot}. Moreover, the results of the 412.8 nm Si II profiles given here are very different from those of the 413.0 nm Si II profiles. The higher order moments (Fig. 18) nor the IPS diagnostics (Fig. 19) help us much. Therefore, the observed intrinsic variations for this star cannot be successfully modeled. Like for HD 140873, we will try to find out if spectral disentangling can improve our results in the near future.

3.7. HD 92287 – HR 4173 – HIP 52043

HD 92287 (m_V = 5.88, B3IV) is the star with the broadest lines in this subsample ($v_{tot} \simeq 80$ km s^{-1}). It is known as a single-lined spectroscopic binary with a circular 2.9-day orbit showing ellipsoidal variations due to the tidal deformation of the primary component (Paper I). Additional variations with
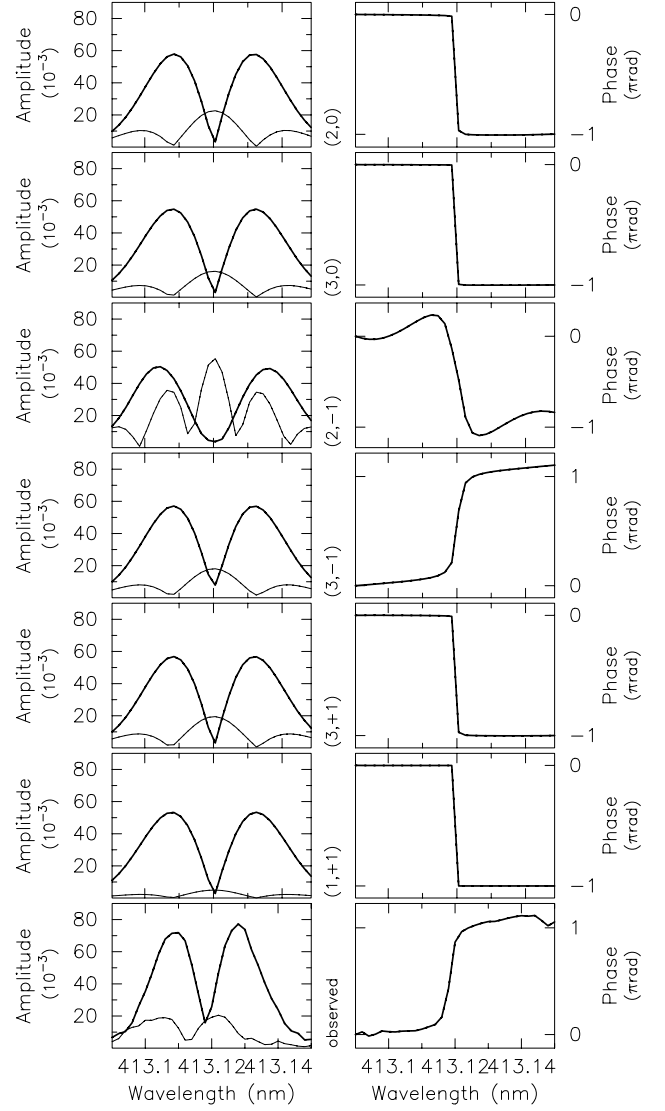

Fig. 16. Same as Fig. 4 but for ν_2 of HD 215573.

Table 5. Same as Table 1, but for ν_2 of HD 215573.

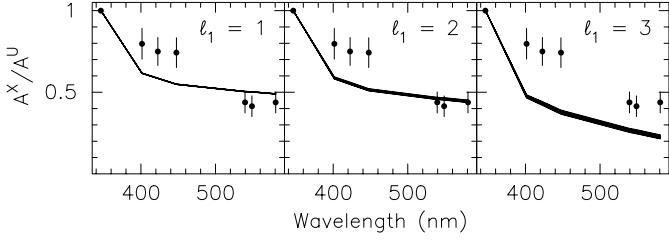| $n°$	ℓ_2	m_2	$\gamma(\ell_2, m_2)$	$A_{p,2}$	$v_{r,max}$	$v_{t,max}$	K_2	i	v_Ω	$\sigma_{413.0}$
1	2	0	8.18	0.44	0.14	0.22	34	67	10	7
2	3	0	8.18	0.17	$\ll$	6.57	34	14	7	8
3	2	−1	8.19	0.57	$\ll$	21.24	48	83	13	4
4	3	−1	8.19	0.33	0.11	3.94	37	48	2	8
5	3	+1	8.21	0.38	0.12	4.16	34	49	0	8
⋮	⋮									
8	1	+1	8.22	1.03	0.36	12.25	34	20	0	8
	2	−1	8.16	0.91	$\ll$	30.65	43	85	9	3
	2	0	8.18	0.44	0.14	0.22	34	67	10	7
	3	0	8.18	0.17	$\ll$	6.57	34	14	7	8
	3	−1	8.20	0.33	0.11	3.95	37	48	2	8
	3	+1	8.21	0.37	0.12	4.16	34	49	0	8
	⋮	⋮								
	1	+1	8.22	1.03	0.36	12.25	34	20	0	8

Fig. 17. Same as Fig. 2, but for $\nu_1 = 0.6054(6)$ c d^{-1} of HD 53921.
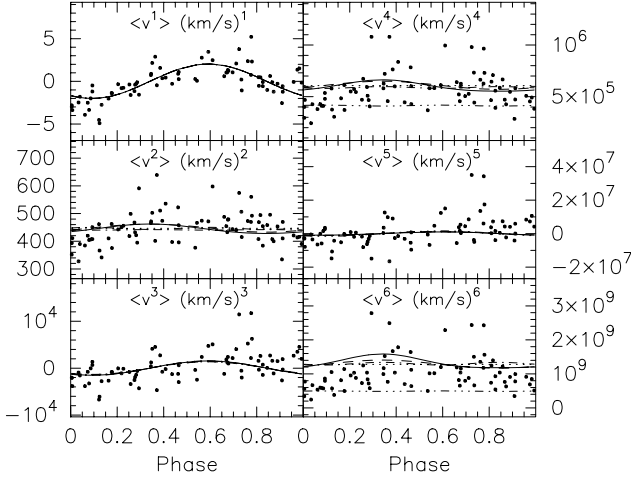
Fig. 18. Same as Fig. 3 but for ν_1 of HD 53921.

Table 6. Same as Table 1, but for ν_1 of HD 53921.

n°	ℓ_1	m_1	$\gamma(\ell_1,m_1)$	$A_{p,1}$	$v_{r,max}$	$v_{t,max}$	K_1	i	v_Ω	$\sigma_{412.8}$
1	3	−3	14.23	0.63	0.26	72.62	92	32	3	16
2	3	−1	14.25	0.48	0.15	12.98	84	4	1	12
3	3	+3	14.25	1.07	0.44	72.52	54	32	0	16
4	3	+1	14.26	0.74	0.24	12.97	54	4	0	12
5	2	0	14.27	0.16	0.05	0.13	54	82	43	3
	3	−3	14.24	0.58	0.24	84.94	116	31	4	16
	3	+3	14.25	1.07	0.44	72.52	54	32	0	16
	3	−1	14.25	0.44	0.15	12.44	84	4	1	11
	3	+1	14.26	0.74	0.24	12.97	54	4	0	12
	2	0	14.27	0.16	0.05	0.13	54	82	43	3

$\nu_1 = 0.2148$ c d^{-1} are prominently present in all our data sets. This *observed* frequency is again very low for an SPB.

The observed amplitude ratios (derived from Table 9 of Paper II) are not fully compatible with the theoretical amplitude ratios found with the error box models, but the best agreement is found for $\ell_1 = 1$ (Fig. 20, left).

The $\langle v \rangle$ variations with ν_1 of the 412.8 nm Si II profiles are clearly non-sinusoidal (Fig. 9 of Paper II). In a theoretical fit, all terms up to the second harmonic of ν_1 have a significant amplitude. Since this non-sinusoidal variation is less prominent in the 413.0 nm Si II profiles, we preferred to use these profiles for the mode identification. The best fitting solutions found with both versions of the moment method are all non-zonal modes (Table 7). Like for most of the other stars, the discriminant values are close to each other. Of the five best fitting solutions
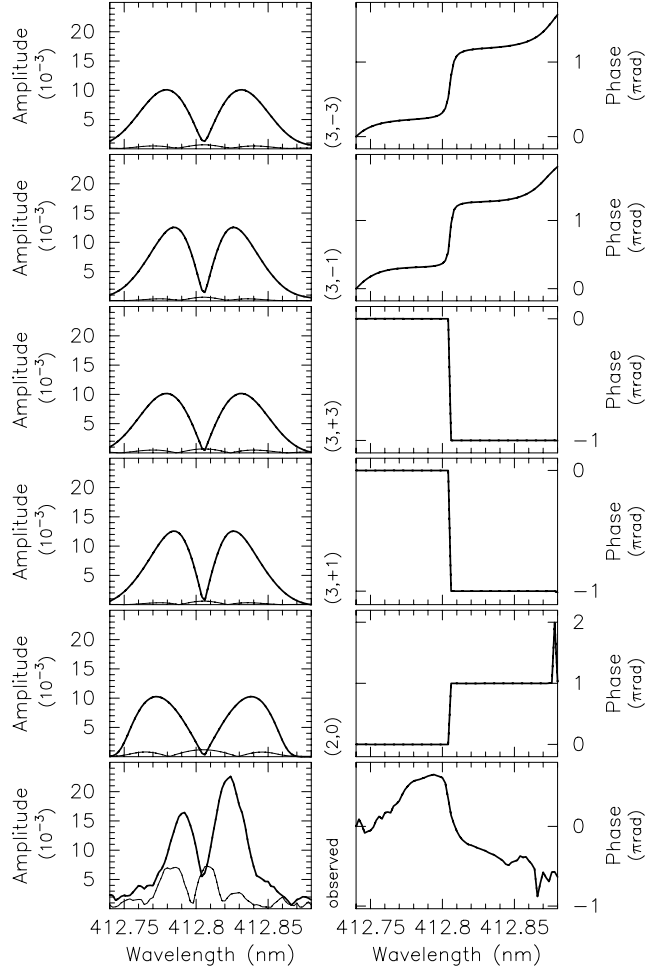

Fig. 19. Same as Fig. 4 but for ν_1 of HD 53921.

with the non-rotating pulsation formalism, the $(\ell_1, m_1) = (1, -1)$ mode is the only one for which both the variations in the higher order moments (Fig. 21) and the amplitude and phase variations across the 413.0 nm Si II profiles (Fig. 22) behave like the observed ones. However, a negative m_1 value leads to a *negative* oscillation frequency in the co-rotating frame. Moreover, unlike the previous targets, the IPS diagnostics of the corresponding $(\ell_1, m_1) = (1, -1)$ mode found with the moment method with the rotating pulsation formalism do *not* bear close resemblance to the observed ones.

We conclude that an $(\ell_1, m_1) = (1, -1)$ mode gives the best fit to our observations when using the standard pulsation theory for spherically symmetric stars. However, the non-sinusoidal $\langle v \rangle$ variations like those observed for the 412.8 nm Si II profiles point towards an inhomogeneous temperature distribution across the stellar surface. The observed frequency therefore could correspond to the rotation frequency. In this case, the primary of HD 92287 would rotate subsynchronously. This target clearly deserves more attention before final conclusions can be drawn.

3.8. Summary

For four of the seven targets with only one observed pulsation mode in the spectroscopic data, i.e. HD 181558, HD 24587,
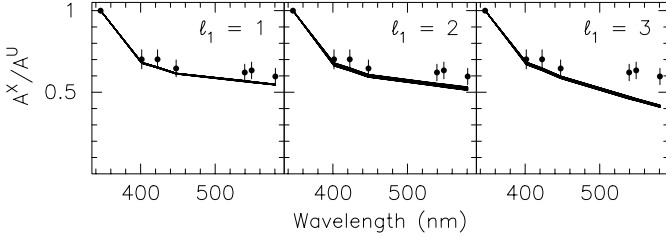
Fig. 20. Same as Fig. 2, but for $\nu_1 = 0.21480(7)$ c d^{-1} of HD 92287.

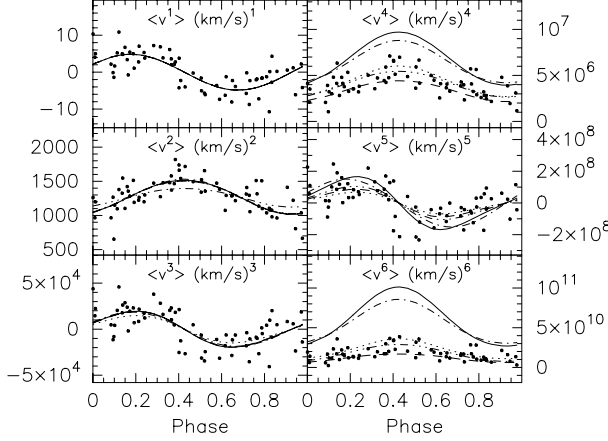

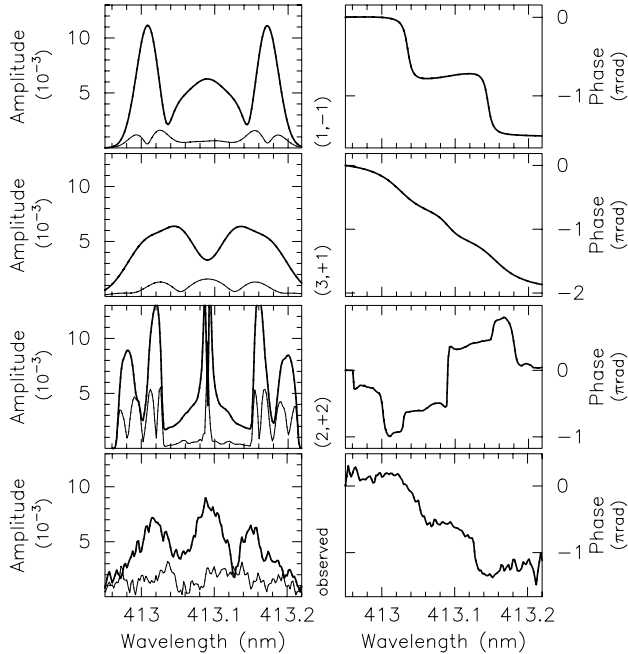**Fig. 21.** Same as Fig. 3 but for ν_1 of HD 92287.

Fig. 22. Same as Fig. 4 but for ν_1 of HD 92287.

HD 140873 and HD 177863, the photometric and spectroscopic identification procedure lead to consistent results (Table 8). Their observed modes are all $(\ell, m) = (1, +1)$ sectoral modes. This is in complete agreement with the theoretical predictions by Townsend (2002). Moreover, such modes are not subject of so-called trapping to the equator, explaining why we see a large dominant amplitude for them (Townsend 2003). Note that the photometric mode identifications performed in Sects. 3.1 to 3.7 were done under the assumption that the observed frequency is

Table 7. Same as Table 1, but for ν_1 of HD 92287.

n°	ℓ_1	m_1	$\gamma(\ell_1, m_1)$	$A_{p,1}$	$v_{r,max}$	$v_{t,max}$	K_1	i	v_Ω	$\sigma_{412.8}$
1	2	+1	25.19	35.66	0.22	107.59	4	3	13	19
2	1	−1	25.20	3.05	1.06	116.68	111	5	8	11
3	3	+2	25.22	8.84	0.07	118.36	13	16	14	12
4	3	+1	25.52	1.45	0.47	6.56	14	37	59	20
5	2	+2	25.54	29.78	11.50	175.55	8	15	19	1
	3	+2	25.30	2.38	0.02	33.34	11	75	57	19
	2	+2	25.58	1.31	0.56	8.77	8	90	72	1
	2	−1	26.08	0.60	0.02	15.14	775	87	9	19
	3	−1	26.13	0.03	≪	127.77	255	67	21	19
	3	−2	26.33	0.67	3.07	111.43	12	17	0	19
	1	−1	26.35	2.18	0.33	17.70	54	5	0	11

equal to the one in the co-rotating frame. We recomputed the results with the co-rotating frequencies listed in Table 8 to check a posteriori how robust the identification is for the changes in the frequency values. In general, we find changes in both the position and the width of the regions of lines of theoretical amplitude ratios for the different ℓ-values indicated in Figs. 2, 5, 8, and 11. However, the overall conclusion, i.e. that $\ell = 1$ is the best fitting photometric mode identification, is confirmed.

For the other three targets, HD 215573, HD 53921 and HD 92287, the results of the identification procedure are inconclusive. Indeed, for HD 215573, the observed photometric variations with ν_2 are compatible with $\ell = 1$ and 2 modes, while all the spectroscopic solutions with ℓ up to 3 are able to explain the observed line profile variations almost equally well. The observations of the pulsating component of HD 53921 are polluted by the light of its visual companion, resulting in unexpected behavior of the observables used in the identification procedures. Spectral disentangling might help for the spectroscopic identification. In case of HD 92287, an $(\ell, m) = (1, -1)$ sectoral mode is able to explain the observed variations, but the corresponding oscillation frequency of the mode in the co-rotating frame is negative, and hence not realistic.

In Table 8, we summarize the values of the maximum radial and tangential surface velocities $v_{r,max}$ and $v_{t,max}$, the continuous parameters i, v_Ω and σ_λ and the derived values of the rotation frequency v_Ω and the ratio of the tangential to radial component of the pulsation velocity K for all the accepted mode identifications. The values of $v_{t,max}$ are 4 to 17 times larger than $v_{r,max}$ and range between 4 and 50 km s^{-1}. For HD 181558 and HD 24587, the differences in the continuous parameters found with the moment method with the rotating and non-rotating pulsation formalism are small. Indeed, we respectively find $v_\Omega \simeq 0.12$ c d^{-1} and 0.40 c d^{-1}. The two v_Ω values found for HD 140873 and HD 177863 differ with a factor of 2 and should therefore not be trusted. However, if we assume for HD 140873 that the stellar inclination equals the orbital inclination of 53° (Paper II) and take $v_{tot} \simeq 75$ km s^{-1} as an upper limit for v_Ω, we find $v_\Omega \leq 0.88$ c d^{-1}. In any case, the primary is rotating super-synchronously. For HD 177863, we could only determine a lower limit of 30° on the orbital inclination (Paper II) which is insufficient for a similar exercise.

Table 8. Overview of the adopted mode identifications (ℓ, m) for the SPBs in the sample of Aerts et al. (1999) with only one observed pulsation frequency ν_{obs} in the spectroscopic data. The stars are given in ascending order of ν_{tot} (km s^{-1}). For the results of both versions of the moment method, we give the values of the maximum radial and tangential surface velocities $\nu_{r,max}$ (km s^{-1}) and $\nu_{t,max}$ (km s^{-1}), the ratio of the tangential to radial component of the pulsation velocity K, the continuous parameters i (°), ν_Ω (km s^{-1}) and σ_λ (km s^{-1}) and the derived value of the rotation frequency ν_Ω (c d^{-1}). For the results of the moment method with inclusion of the Coriolis force, we additionally give the ratio of the equatorial rotation velocity ν_{eq} (km s^{-1}) to the critical velocity ν_{crit} (km s^{-1}), the oscillation frequency in the co-rotating frame ν_{co}, and the "spin parameter" $\eta = 2\nu_\Omega/\nu_{co}$.

Star	ν_{tot}	ν_{obs}	ℓ	m	$\nu_{r,max}$	$\nu_{t,max}$	K	i	ν_Ω	σ_λ	ν_Ω	ν_{eq}/ν_{crit}	ν_{co}	η
HD 181558	25	0.80780	1	+1	1.21	19.73	16	42	12	7	0.127			
					1.65	27.52	17	25	7	3	0.117	0.038	0.925	0.25
HD 24587	40	1.1569	1	+1	0.79	6.26	8	38	32	3	0.426			
					0.53	4.47	8	42	31	5	0.380	0.105	1.537	0.49
HD 140873	75	1.1515	1	+1	2.66	13.61	5	31	69	8	1.226			
					5.50	50.39	9	6	7	12	0.626	0.143	1.777	0.70
HD 177863	75	0.84059	1	+1	2.80	12.64	5	31	67	4	0.921			
					5.89	46.85	8	6	7	10	0.486	0.160	1.326	0.73

For the identifications of the moment method with the rotating pulsation formalism, the ratio of the equatorial rotation velocity ν_{eq} to the critical velocity ν_{crit}, the oscillation frequency in the co-rotating frame ν_{co} and the spin parameter $\eta = 2\nu_\Omega/\nu_{co}$ are additionally listed in Table 8. For all the targets with a well identified mode, we find ν_{eq}/ν_{crit} below 20% and η below 1. The former indicates that we are allowed, in first instance, to ignore the oblateness of the star and the corresponding Von Zeipel effect. The latter justifies the neglect of the Coriolis force in our photometric mode identifications, especially since we are dealing with prograde sectoral modes (Townsend 2003).

4. Conclusions and discussion

We extensively tested some of the latest versions of existing mode identification techniques for a sample of main-sequence *g-mode* pulsators. In this paper (Paper III), we restricted ourselves to the SPBs in the sample of Aerts et al. (1999) for which only one intrinsic frequency is found in our current spectroscopic data sets. The other SPBs in this sample will be discussed in a subsequent future Paper IV. It is rather encouraging that the results of the combined identification techniques tend to converge to a unique identification. We evaluate our 3-step procedure, which is also applicable to the gravity modes present in γ Doradus stars, as follows:

1. The photometric variations were first modeled by using the method of photometric amplitudes using the formalism by Dupret et al. (2003). Contrary to Dupret et al., we did not base our results on *one* theoretical model for each star only. The Liège codes (CLES, MAD) were used to calculate theoretical amplitude ratios for numerous models with metalicity Z and initial hydrogen abundance X fixed to respectively 0.020 and 0.70 and T_{eff} and $\log(g)$ within the observed range for each star. Comparison with the observed amplitude ratios usually led to two possible ℓ values: $\ell = 1$ or 2.

2. The discriminant of the moment method (Briquet & Aerts 2003) was calculated for large grids of pulsation and stellar parameters to find the values giving the best fit to the first three normalized moments of the observed $\lambda\lambda$ 413 nm Si II

profiles. Both versions (without and with inclusion of the Coriolis force) were used. For our targets with $\eta < 0.5$, the differences in the results are small. Also, both Si II lines generally lead to comparable results. We always found several solutions which can fit the observed $\langle v \rangle$, $\langle v^2 \rangle$ and $\langle v^3 \rangle$ variations almost equally well.

3. For the best fitting few moment method solutions, the corresponding synthetic line profiles were calculated with the BRUCE/KYLIE code (Townsend 1997). These were compared with the observed profiles in two ways:

   – We constructed phase diagrams with the observed pulsation frequency for the first *six* normalized moments of both the synthetic and observed line profiles. The use of the diagrams of the *higher order even* moments enabled us to reject some of the competing solutions. To identify *g*-mode pulsations, it would therefore be beneficial to include $\langle v^4 \rangle$ and $\langle v^6 \rangle$ in the calculation of the discriminant of the moment method.

   – For the retained solutions, we compared the synthetic and observed IPS diagnostics, i.e. amplitude and phase variations across the line profile, to pinpoint the best overall fitting spectroscopic (ℓ, m) combination. We could not use the observed *phase difference* across the line profile for a direct estimation of ℓ and m with the formulas given by Telting & Schrijvers (1997, Eqs. (9) and (10)), since they are only applicable to higher degree modes ($\ell > 3$) in rapidly rotating stars ($\nu_\Omega > 5\sigma_\lambda$). For *p*-modes, the total phase differences across a line profile of prograde modes always have the same sign, which is opposite to the sign observed for retrograde modes (Telting & Schrijvers 1997). However, we observed prograde *g*-modes for which the total phase differences across the line profile have opposite signs (e.g. Figs. 4 and 7). Clearly, the moment method in combination with the *amplitude and phase variations* across the whole line profile is a powerful tool to identify low degree *g*-modes.

The results of the photometric identification procedure (step 1) are fully compatible with those of the spectroscopic

identification procedure (steps 2 and 3) for HD 181558, HD 24587, HD 140873 and HD 177863. In these cases, we could conclude that the observed variations are generated by an $(\ell, m) = (1, +1)$ mode (Table 8). For HD 177863, we could not confirm that the observed variations result from a tidally excited $\ell = 2$ sectoral mode (Willems & Aerts 2002).

Two very low frequencies were observed: $\nu_1 = 0.21480(7)$ c d^{-1} for HD 92287 and $\nu_2 = 0.10108(10)$ c d^{-1} for HD 177863 (Paper II). It is not clear if we are dealing with pulsation modes or not. For the corresponding oscillation frequencies in the co-rotating frame to be within the expected range of SPB frequencies, rapid rotation in combination with a *high* and *positive* azimuthal number m are required. However, the identification procedure for HD 92287 converged to a mode with a *low* and *negative* m value. Since variations with $\nu_2 = 0.10108(10)$ c d^{-1} are not present in the observed line profile variations of HD 177863, we were unable to do a detailed identification.

We remind the reader that in our identification procedure, the vibrational stability of the modes was not taken into account. This issue will be discussed in full detail in Paper V.

For a basic seismic study of a β Cephei star, only a few well identified modes are needed (e.g. Aerts et al. 2003; and Pamyatnykh et al. 2004). However, the theoretical frequency spectra of SPBs are much denser than those of β Cephei stars. Moreover, no zonal modes are identified so far. We find indeed observational evidence of a prograde dipole dominant mode. For such modes, one needs to know the rotation frequency ν_Ω to a great accuracy to be able to calculate the oscillation frequency of the mode in the co-rotating frame. However, for mono-periodic cases, the errors on i and ν_Ω found with the moment method are too large for this purpose (De Ridder et al. 2004). At this stage, detailed seismic modeling for SPBs still seems premature. Despite this, we come to the important conclusion that the centrifugal force can, in first instance, be neglected for our target stars. Moreover, during the identification procedure, the effects of the Coriolis force remained unimportant for the stars in which we have obtained a safe mode identification (Table 8) because the spin parameter remains below 1 and because it concerns dipole prograde modes (Townsend 2003). The codes used in this work do not treat effects of mode coupling due to rotation. Future improvements in the theoretical treatment adopted for the photometric mode identification method can be achieved from the work by Daszyńska-Daszkiewicz et al. (2002) and Townsend (2003) but were certainly beyond the scope of the current paper.

References

Adelman, S. J., Robinson, R. D., & Wahlgren, G. M. 1993, PASP, 105, 327

Aerts, C., De Cat, P., Peeters, E., et al. 1999, A&A, 343, 872

Aerts, C., De Pauw, M., & Waelkens, C. 1992, A&A, 266, 294

Aerts, C., Thoul, A., Daszyńska, J., et al. 2003, Science, 300, 1926

Ausseloos, M., Scuflaire, R., Thoul, A., & Aerts, C. 2004, MNRAS, 426

Briquet, M., & Aerts, C. 2003, A&A, 398, 687

Briquet, M., De Cat, P., Aerts, C., & Scuflaire, R. 2001, A&A, 380, 177

Briquet, M., Aerts, C., Lüftinger, T., et al. 2004, A&A, 413, 273

Corbally, C. J. 1984, ApJS, 55, 657

Daszyńska-Daszkiewicz, J. 2005, A&A, in preparation (Paper V)

Daszyńska-Daszkiewicz, J., Dziembowski, W. A., Pamyatnykh, A. A., & Goupil, M.-J. 2002, A&A, 392, 151

De Cat, P. 2001, Ph.D. Thesis

De Cat, P., & Aerts, C. 2002, A&A, 393, 965 (Paper II)

De Cat, P., Aerts, C., De Ridder, J., et al. 2000, A&A, 355, 1015 (Paper I)

De Cat, P., Briquet, M., Daszyńska-Daszkiewicz, J., et al. 2005, A&A, in preparation (Paper IV)

De Ridder, J., Molenberghs, G., & Aerts, C. 2004, Applied Statistics, 54, Part 2, 1

Dupret, M.-A., De Ridder, J., De Cat, P., et al. 2003, A&A, 398, 677

Dziembowski, W. A., Moskalik, P., & Pamyatnykh, A. A. 1993, MNRAS, 265, 588

Gautschy, A., & Saio, H. 1993, MNRAS, 262, 213

Hadrava, P. 1995, A&AS, 114, 393

Hadrava, P. 1997, A&AS, 122, 581

Lee, U., & Saio, H. 1987, MNRAS, 224, 513

Pamyatnykh, A. A. 1999, Acta Astronomica, 49, 119

Pamyatnykh, A. A., Handler, G., & Dziembowski, W. A. 2004, MNRAS, 350, 1022

Schrijvers, C., Telting, J. H., Aerts, C., Ruymaekers, E., & Henrichs, H. F. 1997, A&AS, 121, 343

Telting, J. H., & Schrijvers, C. 1997, A&A, 317, 723

Telting, J. H., Aerts, C., & Mathias, P. 1997, A&A, 322, 493

Townsend, R. H. D. 1997, MNRAS, 284, 839

Townsend, R. H. D. 2002, MNRAS, 330, 855

Townsend, R. H. D. 2003, MNRAS, 343, 125

Wade, R. A., & Rucinski, S. M. 1985, A&AS, 60, 471

Waelkens, C. 1991, A&A, 246, 453

Willems, B., & Aerts, C. 2002, A&A, 384, 441